Anticipatory responses to drought by plants: What are the environmental cues?

Running title:
Anticipating drought

Highlight:
Environmental correlations carry information that plants acquire through sensing.

Pedro J. Aphalo* Victor O. Sadras†

Draft of: September 29, 2021

Figures: 11 + 14, all in colour. Tables: 1. Cited works: 58. Words: xx (excluding citations and methods).

*Organismal and Evolutionary Biology Research Programme, Viikki Plant Science Centre, Faculty of Biological and Environmental Sciences, University of Helsinki, Finland. mailto:pedro.aphalo@helsinki.fi, tel. +358 50 3721504
†South Australian Research and Development Institute, and School of Agriculture, Food and Wine, The University of Adelaide, Australia. mailto:victor.sadras@sa.gov.au

Abstract (213 words)
This study is an attempt to reconcile the physics-driven variation in reference evapotranspiration (ET_0) and possible sensory-driven anticipatory acclimation that contributes to tolerance of dry weather spells and drought by plants growing in open fields. We use an original data set measured at high temporal resolution. These data include the standard meteorological observations plus detailed observations of different bands of sunlight: UV-B, UV-A, photosynthetically active and global down-welling short-wave radiation, blue, red and far-red light from two growth seasons at Helsinki, Finland. We also report ET_0 computed with the FAO formulation of the Penman-Monteith equation. We assessed the correlations among variables at different time scales and their performance as predictors of ET_0. We conclude that all studied bands of sunlight are consistently good predictors of ET_0. UV radiation is a specially good predictor of the daily course of ET_0 while longer wavelengths function better in the prediction of day to day variation in ET_0. In most cases sunlight bands that plants are known to sense through specific photoreceptors can explain more than 95% of the variation in ET_0, making them as cues carrying information on the demand side of the water budget of vegetation. Sunlight as sensed by plants is consequently a good candidate as driver of anticipatory acclimation to likely future drought events.

Keywords: drought, sunlight, anticipation, acclimation, cue, signal, plants, transpiration, evaporation, weather.

Abbreviations: PAR = photosynthetically active radiation, $400\,\text{nm} < \lambda < 700\,\text{nm}$; R = red light, $655\,\text{nm} < \lambda < 665\,\text{nm}$; FR = far-red light, $730\,\text{nm} < \lambda < 740\,\text{nm}$; UV radiation, $280\,\text{nm} < \lambda < 400\,\text{nm}$; UV-B radiation, $280\,\text{nm} < \lambda < 315\,\text{nm}$; UV-A 2 radiation, $315\,\text{nm} < \lambda < 340\,\text{nm}$; UV-A 1 radiation, $340\,\text{nm} < \lambda < 400\,\text{nm}$; ET = evapotranspiration, evaporation + transpiration, ET_0 = potential or reference evapotranspiration.

1. Introduction

This study is an attempt to reconcile the physics-driven variation in reference evapotranspiration (ET_0) and possible sensory-driven anticipatory acclimation that contributing to tolerance of dry weather spells and drought by plants growing in open fields.

The scaling of water fluxes from plants to fields and regions was a subject of intense research in the 1980s. It was then concluded that over large land surfaces the main driver of evapotranspiration (ET) is available energy when surface resistance is low and water supply unrestricted. These are conditions assumed for the calculation of potential- or reference evapotranspiration (ET_0), as discussed by McNaughton (1989). In contrast actual evapotranspiration (ET) is not restricted to these idealized conditions, and usually less than ET_0.

The Penman-Monteith equation, (1), is an accepted method for estimation of ET based on the mechanisms of energy and matter exchange,

$$\mathrm{ET} = \frac{\Delta(R_\mathrm{n} - G) + \rho_\mathrm{a} c_\mathrm{p} (e_\mathrm{a}^* - e_\mathrm{a})/r_\mathrm{a}}{(\Delta + \gamma(1 + \frac{r_\mathrm{s}}{r_\mathrm{a}}))\rho_\mathrm{w}\lambda} \tag{1}$$

where ET is the evapotranspiration flux, Δ the slope of the saturation vapor pressure vs. temperature curve, R_n the net radiation flux density, G the sensible heat flux density into the soil, ρ_a the air density, c_p the specific heat of moist air at constant pressure, e_a^* the saturation water vapor pressure at air temperature, e_a the actual water vapor pressure of the air, r_a the aerodynamic resistance to turbulent transfer from the surface to some z height above the surface, γ the pyschrometric constant, r_s the bulk surface resistance to flow of water vapor from inside the leaf, vegetation canopy or soil to outside the surface, ρ_w the density of liquid water, and λ is the latent heat of vaporization.

The simplified formulation from FAO's publication No. 56 and its revisions combines equation (1) with those for r_a, ρ_a and λ (Allen et al., 2006),

$$\mathrm{ET}_0 = \frac{k_\mathrm{e}\Delta(R_\mathrm{n} - G) + \gamma\frac{k_\mathrm{n}}{T_\mathrm{a}+273}u_2(e_\mathrm{a}^* - e_\mathrm{a})}{\Delta + \gamma(1 + k_\mathrm{d}u_2)} \tag{2}$$

where k_i are numeric constants with values that depend on the time step of the

computations and the units of the input data, u_2 wind speed at 2 m, T_a air temperature at 2 m (°C), and all other symbols as in equation (1).

As a result of validation studies, ASCE-EWRI updated equation (2) by adjusting the numerical values of the k_i constants, both for the same hypothetical grass sward canopy as used for ET_0 according to FAO56 and for a 0.5 m-tall canopy similar to a field of alfalfa (Allen et al., 2006). In this updated version the value of k_d is different for day and night. Although the formulation is fixed, how calculations are done depends on the available data. There are procedures specified for the estimation of missing data for some of the inputs.

Equations (1) and (2) are mechanistically based on the energy balance of the foliage, transfer resistances and concentration gradients. Use of equation (2) is restricted to large areas of uniform vegetation while equation (1) is not, as long as values for s and a are available. The values used for the numeric constants k_i are based on various assumptions about the vegetation and as well as that g_l^w is high and that soil water is not limiting. It treats the canopy as an imaginary "big leaf" representing the foliage as a whole. The resistance to the flow of water vapour is described by two resistances in series, the surface resistance of the canopy (r_s) and the aerodynamic resistance (r_a) affect water vapour transport into the air above the canopy's boundary layer. r_a is a function of the wind speed and roughness of the canopy. In the case of ET_0, r_a is computed assuming a uniform grass sward 0.12 m tall and r_s assumed to be low during daytime reflecting high g_l^w.

Even when considering non-idealized canopies and conditions, available energy remains a key determinant of ET. This is in contrast to the central role of stomata in the regulation of transpiration of an isolated plant under controlled conditions (Jarvis and McNaughton, 1986). So, even though ET_0 and ET are calculated using a "big leaf" approximation involving similar terms as the calculation of transpiration from an individual leaf, the main variables governing water flux are depend on the spatial scale (Jarvis, 1985; Jarvis and McNaughton, 1986; Campbell and Norman, 1998). In brief, assuming that only a single leaf responds to its environment leads to different conclusions than assuming that all leaves in a field or forest respond concurrently to an external change in the environment. The process of estimating ET from responses of leaf conductance (g_l^w) or of transpiration by individual leaves (E) is an scaling-up problem rather

than a simple summation problem because of feedbacks loops. What is different for ET and E is the boundary of what we consider the system of interest and consequently the height z where we can assume that conditions remain unaffected by changes in the water vapour flux rate we are studying or estimating: outside the leaf boundary layer for E vs. above the regional boundary layer for ET.

With a focus on an individual plant or leaf, stomatal conductance is critical to the regulation of water use, but for a field of short vegetation not limited by water supply, differences in stomatal conductance among individuals mainly affect how these individuals share the total water flux, which is mainly dependent on the energy input (Aphalo, 1991). In the case of ET, $g_{\mathrm{l}}^{\mathrm{w}}$ is only one component of r_{s} as evaporation may also take place at the soil surface or on wet plant surfaces (usually $r_{\mathrm{a}} > r_{\mathrm{s}}$); r_{s} depends in addition on the leaf area index (LAI) because it is expressed per unit ground area as is ET, while $g_{\mathrm{l}}^{\mathrm{w}}$ is expressed per unit leaf area. The interception of radiation by the foliage depends on the spatial distribution of leaves and their positions, as well as on LAI. However, the assumption for ET_0 is that all incoming radiation is intercepted by foliage and that the albedo is 0.23, i.e., that 23% of incoming solar radiation ($\lambda < 4000\,\mathrm{nm}$) radiation is reflected back and 77% absorbed .

Drought as a meteorological phenomenon of abnormally low water availability is in most cases a regional phenomenon, dictated by the spatial distribution of rainfall. From a plant physiology perspective the water budget is dependent on the soil characteristics, topography, timing and previous environmental conditions experienced. In general we need to distinguish between drought and stress, as stress is related to each individual plant. Acclimation, the adjustment of physiology, morphology and development to the circumstances can delay or mitigate stress during a drought spell. Definitions of acclimation vary to some extent, but in all cases plastic responses are assumed to take time and to be mostly irreversible or only very slowly reversible. These features of acclimation indicate that to be effective, acclimation needs to be anticipatory (Novoplansky, 2016). Anticipation implies that plants perceive the environmental conditions they are likely to experience in the near future (Aphalo and Sadras, 2021).

1.1. Daylight carries information

Mechanisms for the acquisition of information are characteristic of all organisms, from bacteria to humans, including plants (Capra and Luisi, 2014). These mechanisms contribute to fitness because they allow anticipatory behaviour (Novoplansky, 2016). An important question from the perspective of sensory ecology is what are the available sources of information an organism has access to and that could guide a given anticipatory response.

Sensing of light through wavelength-selective photoreceptors allows acquisition of information (Smith, 1981b; Novoplansky et al., 1990; Aphalo and Ballaré, 1995). Daylight carries information through changes in its spectrum and in its irradiance (Aphalo and Ballaré, 1995; Casal, 2013) as well as the seasonality of the photoperiod, sensed by plants as the length of the night through photoreceptors (Song et al., 2015). Variables in the environment carry a wealth of information as a result of temporal and spatial auto-correlations and cross-correlations (Aphalo and Sadras, 2021).

The spectral composition of sunlight varies with sun elevation, as the shorter wavelengths of UV are depleted when the sun is low in the sky (Aphalo et al., 2012). The photon ratio between $Q_{\text{UV-B}}$ and Q_{PAR} varies strongly during the course of the day and with time of the year, specially at high latitudes (Kotilainen et al., 2020) but is only moderately affected by clouds (Lindfors and Arola, 2008). Within canopies, a situation not considered in detail here, the R:FR photon ratio depends very strongly on the leaf area overhead and to a lesser extent on the plant species imposing shade (Holmes, 1981; Hartikainen et al., 2020; Durand et al., 2021). The R:FR is also affected by differential reflection of FR by green vegetation, so it changes before shading by neighbours starts (Ballaré et al., 1990). In addition, the R:FR depends weakly on the solar elevation angle and the water column in the atmosphere (Kotilainen et al., 2020). This causes some variation during the course of the day, through the seasons of the year and with latitude even at the top of a canopy (Smith and Morgan, 1981; Kotilainen et al., 2020).

The shorter wavelengths are more scattered in the atmosphere than the longer wavelengths of the spectrum (Lindfors and Ylianttila, 2016), so UV radiation penetrates more readily into vegetation canopies (Durand et al., 2021) than blue

and red light, although they are all three strongly absorbed by the leaves of most plants.

We hypothesise that plants can anticipate and acclimate to drought by sensing evaporative demand (measurable as ET0) or a variable correlated with it. This hypothesis is justified by the fact that in the absence of restrictions to water supply, the rate at which the water stored in the soil is being depleted is proportional to ET_0. For vegetation ET_0 represents a ceiling for actual ET (Campbell and Norman, 1998). As far as we know plants cannot directly sense ET_0 or water loss at field scale. However, plants can sense different wavelengths of sunlight, temperature and $e^* - e$. We may then ask if any of these variables can functions as proxies for ET_0 and at which temporal scales.

1.2. Variables sensed by plants

Plants have multiple photoreceptors that allow them to separately sense different wavebands of the solar spectrum (Paik and Huq, 2019). Furthermore, signalling downstream of these photoreceptors is interconnected leading to complex interactions (Moriconi et al., 2018; Rai et al., 2021). The wavebands considered most important are UV-B (280–315 nm), UV-A (315–400 nm), blue (400–500 nm), red (655–665 nm) and far-red (730–740 nm).

Temperature responses in plants are not only the result of the effect of temperature on overall metabolic- and biochemical-reaction rates, but temperature is like light sensed and used as a source of information that triggers specific responses (Hayes et al., 2021). The R and FR photoreceptor phytochrome B and the UV-A/B photoreceptor phototropin are among plants' direct temperature sensors (Casal and Qüesta, 2018; Hayes et al., 2021).

Stomata are sensitive to water vapour, probably through multiple mechanisms, including the bulk rate of transpiration (Monteith and Unsworth, 2008) and sensing of VPD, possibly through localized evaporation and long distance signalling (Aphalo and Jarvis, 1991; Mott and Parkhurst, 1991; Monteith, 1995; Buckley, 2005; Peak and Mott, 2011).

Plants can also perceive mechanical stimuli including wind, touch and vibrations (Telewski, 2006). Repeated exposure to wind can result in shorter plants while

touching leaves or shaking them can induce stomatal closure.

On the other hand, there is evidence that at least under some conditions, pre-exposure to solar UV-B and/or UV-A radiation can trigger acclimation leading to enhanced tolerance and even stress avoidance during a subsequent drought event (Gitz and Liu-Gitz, 2003; Robson et al., 2016). This has been frequently attributed to stress from UV exposure enhancing tolerance to drought stress (e.g. Bandurska et al., 2013). Two non-mutually exclusive mechanisms can underly this response: UV as a stress factor, and UV as a cue. Current consensus is that exposure to solar UV radiation only exceptionally induces stress in plants growing in the field (Robson et al., 2019). Furthermore, recent results support the idea proposed by Gitz and Liu-Gitz (2003) that induction of stress by UV radiation is not necessary for preemptive acclimation that protects from drought induced stress (Yan, 2021). Solar UV-B and/or UV-A 2 radiation can function as a source of information, sensed by plants through the UVR8 photoreceptor (Rai et al., 2021) and induces acclimation that delays or moderates the development of stress under water restriction (Yan, 2021). Furthermore, responses mediated by UVR8 are negatively modulated by UV-A 1 and blue radiation sensed through the cryptochrome photoreceptors (Rai et al., 2020; Tissot and Ulm, 2020; Rai et al., 2021). However, the common proposition that UV-B radiation is a good predictor of drought remains speculative. In particular, no previous study has considered this problem in the light of the sensory capabilities of plants or at multiple time scales.

1.3. Aims of the study

Given that available energy is the main driver of ET_0, we hypothesized that UV-B radiation and/or some other components of solar irradiance are good sources of information about current ET_0 and accessible to plants. However, as plants can sense also temperature, wind and air humidity, we also included these variables in the study given that they are mechanistically linked to ET_0.

Our aim was to compare the effectiveness of these variables in their hypothetical role as predictors of ET_0 by assessing regressions and cross-correlations.

2. Methods

2.1. Data and its acquisition

Original data with high temporal resolution and discriminating different bands of the solar spectrum were collected at a research-oriented weather station located in the experimental field at the Viikki campus of the University of Helsinki, Finland (25.01673 E, 60.2253 N, 8 m a.s.l.). These data describe the daily course as well as seasonal variation in the environmental conditions during the growing season in two consecutive years.

The data were acquired with a datalogger (CR6, Campbell Scientific, Logan, UT, USA) expanded with an analogue input module (CDM-A116, Campbell Scientific), powered by a battery charged in parallel from mains power and solar panels. Except for those in the soil, sensors are mounted onto a 3-m tall galvanized-steel instrument tripod (CMxxx, Campbell Scientific). The data reported are for the period 7 May 2020 to 28 September 2021, excluding data from 1 November 2020 to 31 March 2021, the winter period. Data were collected also through the winter but radiation data are suspect for this time of the year due to the intermittent accumulation of snow on the broadband sensors. The sensors in the station are listed in Table 1. Most measurements were acquired once every 5 s and means of 12 values logged at 1 min intervals. The exception are data from the soil at 0.05 m and deeper depths that were acquired and logged once per hour (data not shown). Wind speed and direction, air temperature, air humidity, precipitation and atmospheric pressure were measured at a height of 2 ± 0.3 m.

All visible and UV radiation sensors were calibrated simultaneously while deployed on site by comparison to a recently calibrated array spectrometer (Maya 2000 Pro, Ocean Optics, now Ocean Insight, Orlando, FL, USA). Spectral data were acquired with R (R Core Team, 2021) and package ‘ooacquire’ (Aphalo and Ylianttila, 2021) using an improved version of the protocol described in (Ylianttila et al., 2005) (method `"ylianttila.mthd"` in ‘ooacquire’). The integration time was optimized to attain at the peak $95 \pm 3\%$ of the maximum detector counts and the number of integrations adjusted to maintain a constant combined integration time of at least 10 s. Integration time was “bracketed” to improve the dynamic range and the resulting spectra spliced, with the low signal

Table 1: Variables in the high temporal resolution data set and their origin. *n.a.* indicates not applicable. The WXT-520 sensor was replaced by a WXT-530 in April 2021. Acq. = data acquisition frequency; Logg. = data logging frequency; Q = photon irradiance, I = energy irradiance, T = temperature, e = water vapour pressure; u = horizontal wind speed; $\vec{u}$ = wind direction; P_{atm} = atmospheric pressure; p_{rain} = rain precipitation; w = volumetric water content; ET_0 = reference evapotranspiration. Subscripts: UV-B = ultraviolet B radiation (250–315 nm); UV-A = ultraviolet A radiation (315–400 nm); B = blue light (400–500 nm); R = red light (655–664 nm); FR = far-red light (730–740 nm); PAR = photsynthetically active radiation (400–700 nm); SW = short-wave radiation (280–4000 nm).

Variable	Acq.	Logg.	Technique	Sensor type	Make
$Q_{\text{UV-B}}$	5 s	$\bar{x}$, 1 min	SiC photodiode	SEN2-UVB-Cosine	sglux
$Q_{\text{UV-A}}$	5 s	$\bar{x}$, 1 min	SiC photodiode	SEN2-UVA-Cosine	sglux
Q_{B}	5 s	$\bar{x}$, 1 min	GaP photodiode	SEN2-Blue-Cosine	sglux
Q_{R}	5 s	$\bar{x}$, 1 min	Si photodiode	SKR-110	Skye
Q_{FR}	5 s	$\bar{x}$, 1 min	Si photodiode	SKR-110	Skye
Q_{PAR}	5 s	$\bar{x}$, 1 min	Si photodiode	LI-190	LI-COR
$Q_{\text{PAR,diff.\&tot.}}$	5 s	$\bar{x}$, 1 min	Si	BF5	Delta-T
I_{sw}	5 s	$\bar{x}$, 1 min	thermopile	SMP3	Kipp
T_{air}	< 5 s	$\bar{x}$, 1 min	PT100	WXT-520/536	Vaisala
e_{air}	< 5 s	$\bar{x}$, 1 min	HUMICAP	WXT-520/536	Vaisala
u_2	0.25 s	$\bar{x}$, 1 min	2D sonic	WXT-520/536	Vaisala
$\vec{u}_2$	0.25 s	$\bar{x}$, 1 min	2D sonic	WXT-520/536	Vaisala
P_{atm}	< 5 s	$\bar{x}$, 1 min	BAROCAP	WXT-520/536	Vaisala
p_{rain}	1 min	$\sum x$, 1 min	sonic	WXT-520/536	Vaisala
T_{surface}	5 s	x, 1 min	IR 8–12 μm	OPT-CSMV-LT02	Optris
$T_{\text{soil,z}}$	1 h	x, 1 h	thermistor	SoilVue	Campbell
$w_{\text{soil,z}}$	1 h	x, 1 h	TDR	SoilVue	Campbell
ET_0	1 min	*n.a.*	calc.	Penman-Monteith	*n.a.*
solar time	1 min	*n.a.*	calc.	Meeus	*n.a.*

regions coming from spectra measured using $\times 10$ the base integration time. For each spectrum, measurements under three conditions were taken within not more than 2 min: a light measurement, a light measurement with a filter blocking UV radiation ($\lambda \leq 400\,\text{nm}$), and a dark measurement. This protocol together with a special calibration protocol and matching algorithm allow correction for stray light, slit function and increase the dynamic range. This makes it possible to measure UV-B radiation in sunlight reliably. As entrance optics a high performance cosine diffuser (D7-H-SMA, Bentham, Reading, U.K.) connected with an optical fibre (xxxx, Ocean Optics) and mounted on a custom-made levelling base were used. The distance between this entrance optics and the broadband sensors calibrated was less than 10 m. During measurements the operator ducked down and remained at least 5 m away, on the side opposite to the sun. Other sensors were factory calibrated.

The observed data were used to estimate ET_0 for a short (0.12 m-tall) vegetation canopy at 1 min intervals. We used the FAO56 formulation of the Penman-Montieth equation, as modified by ASCE (ASCE-PM short canopy) (Allen et al., 2006). Given the availability of measured atmospheric pressure (P_{atm}) the psychrometric constant (γ) was computed from it instead of assumed constant. Soil heat flow was assumed to be negligible. Functions `ET_ref()`, `ET_ref_day()`, `water_vp_sat()`, `water_vp_sat_slope()`, `psychrometric_constant()` and `net_radiation()` from R package 'photobiology' version 0.10.7 (Aphalo, 2015) were used to compute ET_0.

Local solar time, the position of the sun in the sky and day length were also computed using a re-implementation in R package 'photobiology' (Aphalo, 2015) of Meeus' equations (Meeus, 1998) as used in NOAA's on-line web calculator.

All calculations of solar radiation summaries were done in R 4.1.0 or 4.1.1 (R Core Team, 2021) with packages 'photobiology' (Aphalo, 2015), 'dplyr' (Wickham et al., 2021) and 'lubridate' (Grolemund and Wickham, 2011). The data from the logger were imported into R with the help of R package 'photobiologyInOut' (Aphalo, 2015). Plots and the model fits they contain were created in R with packages 'ggplot2' (Wickham, 2016) and 'ggpmisc' (Aphalo, 2021).

2.2. Data analysis

The relative importance of the different variables entering the ET_0 calculation was assessed by the `"lgm"` method as implemented in R package 'relaimpo' (Grömping, 2006) in a linear model with ET_0 as response variable and I_{sw}, T_{air}, $e^*_{air} - e_{air}$ and u as explanatory variables. The lgm approach is based on R^2 partitioned by averaging over orders and computed by numerical approximation. We did quantile regression fits with R package 'quantreg'. We made also use of R packages 'nlme' (Pinheiro et al., 2021), 'tibble' (Müller and Wickham, 2021), 'dplyr' (Wickham et al., 2021) and 'tidyr' (Wickham, 2021).

We built correlation matrices for these variables together with solar radiation in those bands known to be perceived through plant photoreceptors, to not only detect possible proxies for potential evapotranspiration rate, but also assess the collinearity among variables entering the ET_0 calculations. The matrices were plotted with variables grouped according to hierarchical clustering using R package 'ggcorrplot' (Kassambara, 2019).

Given that the main focus of the study was to assess what sources of information plants could use to "forecast" future drought and/or heat stress events, we assessed the goodness of different variables as predictors of ET_0. We used polynomial regression fitted by ordinary least squares (OLS) and compared the adjusted coefficients of determination (R^2_{adj}). We used R^2_{adj} instead of R^2 because the number of parameters was not the same in all the fitted models. In spite of this, small differences in R^2_{adj} must be interpreted with caution.

Given the high frequency of data acquisition over two whole growing seasons, by doing the analyses described above on the original observations and on their averages when grouped by calendar day or by time of day we assessed the correlations at different time scales.

3. Results

3.1. Drivers of evapotranspiration

The Penman-Monteith's (PM) equation we used to compute ET_0 is an approximation based on the Physics processes regulating the water flux. This equation takes as input radiative energy, air temperature and water vapour pressure deficit as well as wind speed and atmospheric pressure. Atmospheric pressure plays a minor role in the calculations and is frequently ignored.

An initial question before considering proxies, is to analyse how much reference evapotranspiration depends on each of the different variables used as input in its estimation. The importance of the variables depends on their variation and correlations, so we used for this analysis the same data we later used to the search for proxies of ET_0 that plants could sense and use as sources of information. The apparent importance of the variables also depends on the model fitted. We selected a simple model that is able to give a very good fit to the data.

$$\widehat{\mathrm{ET}_0} = b_0 + b_1 \cdot I_{\mathrm{sw}} + b_2 \cdot T_{\mathrm{a}} + b_3 \cdot (e^*_{\mathrm{a}} - e_{\mathrm{a}}) + b_4 \cdot u_2 + \epsilon_{ij} \quad (3)$$

We considered correlation corresponding to three different types of temporal variation: those revealed by 1) the original observations at a 1 min time step, 2) daily summaries, and 3) monthly means for each hour of the photoperiod. Our aim was to investigate whether short-term and long-term correlations are consistent.

In all analyses we used data for the period from April to September, as at our location, at other times of the year snowfall and snow on the ground may be present. Except for daily totals, we consider only data for sun elevation angles of 5 degrees or more as the rate of evapotranspiration is much lower at night.

For the original observations at 1 min time step, the energy input is most important towards explaining variation in evapotranspiration, contributing between 82% and 71% of the R^2. Depending on the month of the year, wind speed and vapour pressure deficit alternate as second in importance, while in most cases temperature makes only a small contribution (Fig. 1).

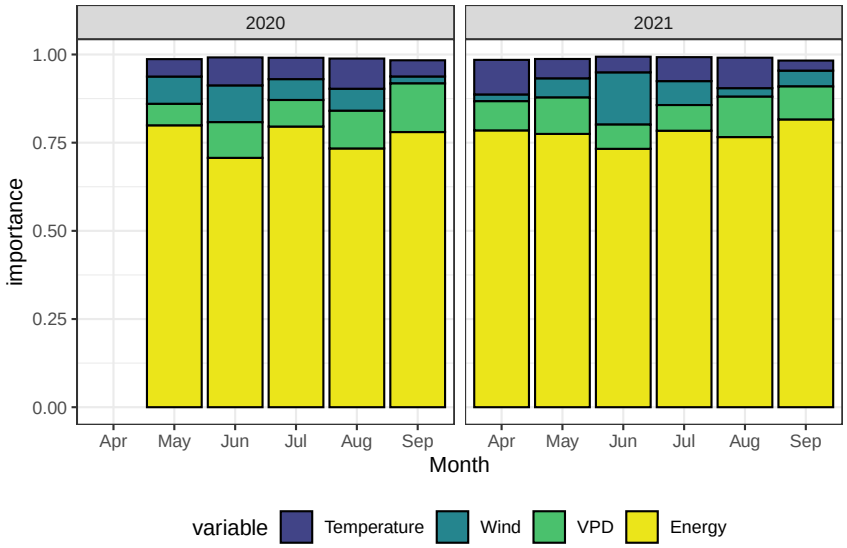

Figure 1: Relative importance of variables in the computation of ET_0 on a 1 min time step. The total R^2 of the fitted linear model is partitioned based on the contribution of different variables. The stacked bar displays the R^2 for each fit, with in all cases $R^2 > 0.98$. n = 274075.

For daily totals, energy and vapour pressure deficit remain as main drivers of evapotranspiration. Month to month variation in the relative importance is, however, larger than for the original observations (Fig. 2).

For monthly means for each hour of the photoperiod (based on local solar time), relative importances are rather different than on a 1 min or an daily time steps, with the importance of wind speed increasing and that of global radiation decreasing. The four variables taken together still explain almost all variation in ET_0 with $R^2 > 0.99$ for all months (Fig. 3).

3.2. Correlations

The input variables to the Penman-Monteith equation can be strongly cross-correlated as for example, water vapour pressure tends to vary little through the course of a day and consequently changes in the vapour pressure deficit are dependent on air temperature. As a result, $e^* - e$ is at its maximum in the early afternoon when air temperature is highest. Correlations for the original observations logged at 1 min interval are all positive and very strong among all

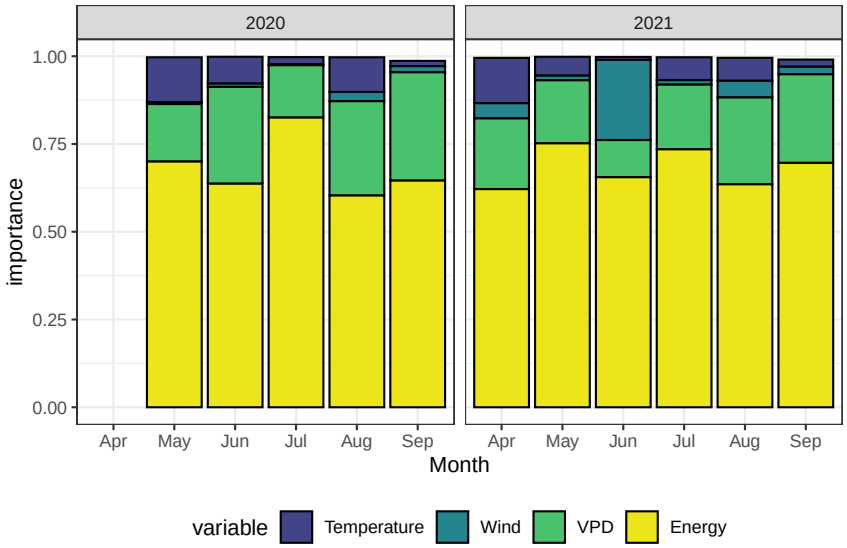

Figure 2: Relative importance of variables in the computation of ET_0 on a daily time step. The total R^2 of the fitted linear model is partitioned based on the contribution of different variables. The stacked bar displays the R^2 for each fit, with in all cases $R^2 > 0.99$. n = 317.

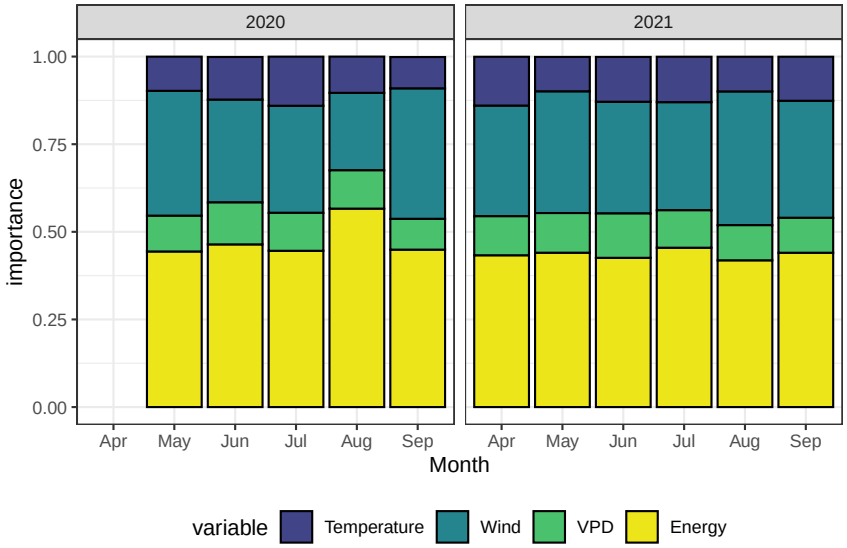

Figure 3: Relative importance of variables in the computation of hourly ET_0 on an hourly time step. The total R^2 of the fitted linear model is partitioned based on the contribution of different variables. The stacked bar displays the R^2 for each fit, with in all cases $R^2 > 0.99$. n = 155.

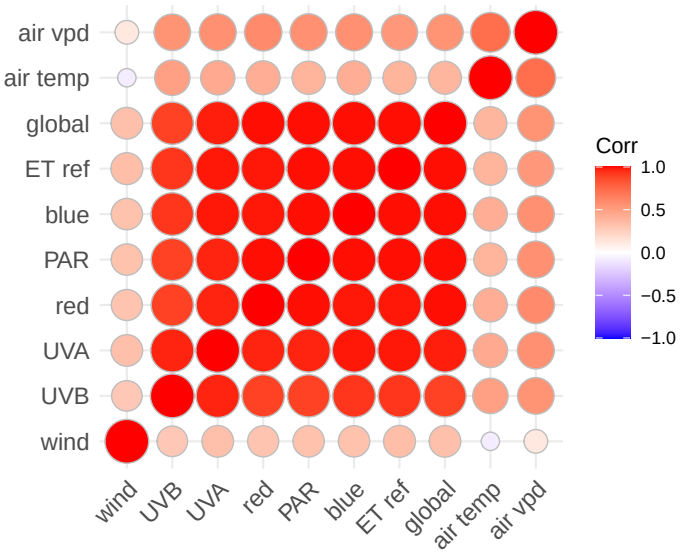

Figure 4: Correlation matrix for observations logged at 1 min intervals for sun elevations equal or higher than 5 degrees. n = 274072. Variables are clustered based on the similarity of the correlation patterns.

pairs of sunlight wavebands and for ET_0 against each of them (Fig. 4). Correlations involving wind speed, air temperature or $e^* - e$ are much weaker.

Correlations in day to day variation are shown as a correlation matrix for daily means (Fig. 5). In this case wind speed is very weakly and negatively correlated with ET_0 and solar radiation bands, while air temperature and $e^* - e$ are positively with each other and with solar radiation. As for observations at 1 min time step, the different bands of sunlight and ET_0 cluster together.

Correlations within the average daily course are shown as a correlation matrix for monthly means for each hour of the day (Fig. 6). The clustering suggests that the correlations during the daily course of the photoperiod are slightly different, with a larger importance of wind speed than for day to day variation.

At all three time scales the different bands of sunlight and ET_0 cluster together, and consistently global radiation is an immediate neighbour of ET_0. The ordering based on R^2 within this cluster varies, but given that correlation coefficients are consistently very high among this group of variables, this variation is mostly inconsequential.

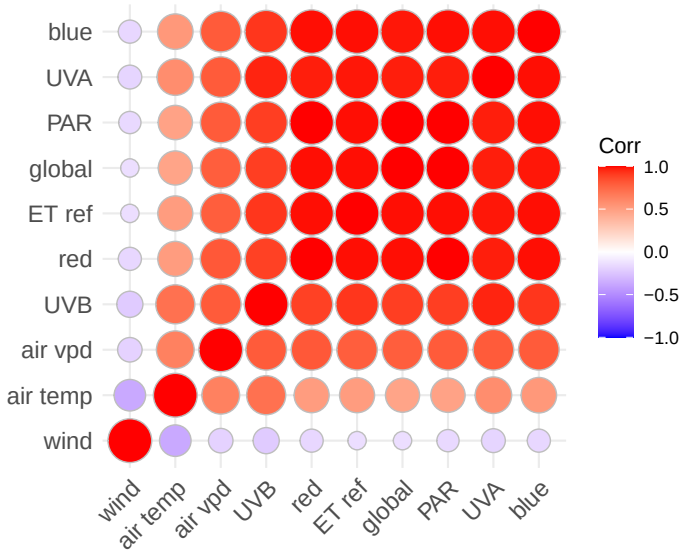

Figure 5: Correlation matrix for daily means from observations logged at 1 min intervals through 24 h. n = 317. Variables are clustered based on the similarity of the correlation patterns.

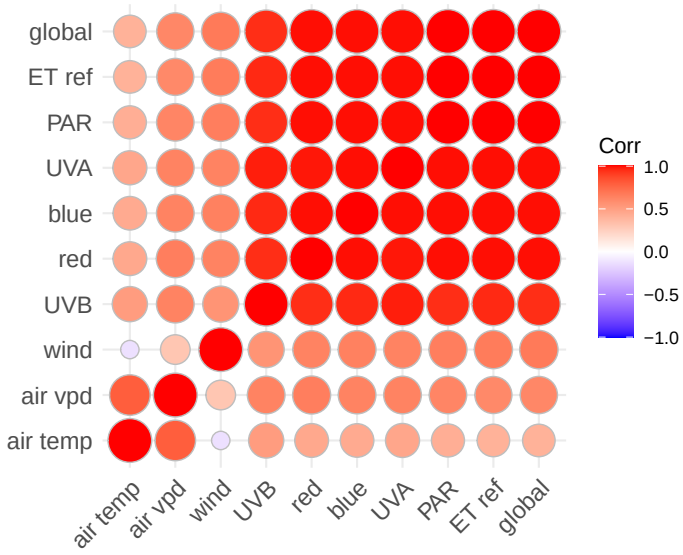

Figure 6: Correlation matrix for monthly means for each our of the day, from observations logged at 1 min intervals through 24 h. n = 155. Variables are clustered based on the similarity of the correlation patterns.

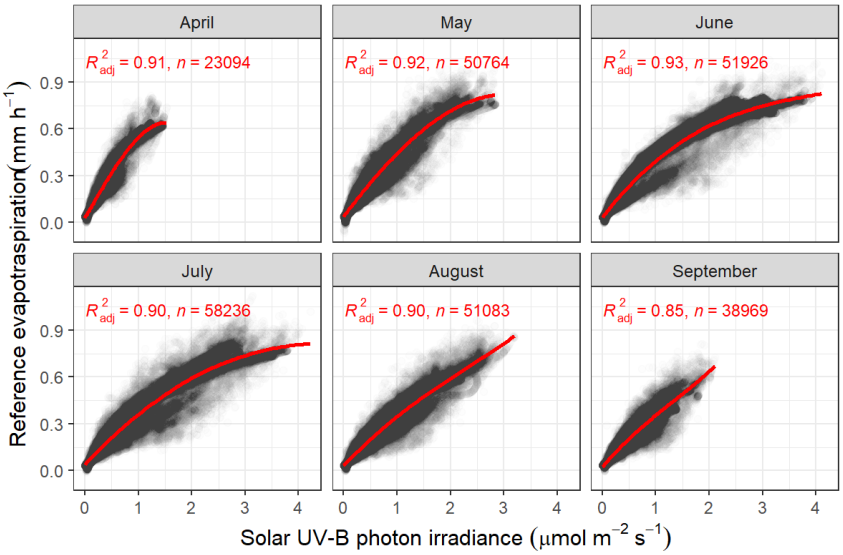

Figure 7: Relationship between reference evapotranspiration for a short vegetation cover (ET_0) vs. UV-B photon irradiance ($Q_{UV\text{-}B}$). Observations are means logged at 1 min interval. In red fitted 3rd degree polynomial. Observations are plotted as semi-transparent dots (black corresponds to 125 or more overlapping points).

3.3. Proxies for ET_0

Until now we have considered linear correlation and linear fits. These yielded slightly smaller estimates of correlation coefficients between UV-B radiation and ET_0 than for other bands of the solar spectrum. We need however to consider that within the photoperiod the relationship between global irradiance and UV-B irradiance is not linear while the relationship for UV-A 1 and longer wavelengths is almost perfectly linear (cf. Figs. 24 and 25). This results in a curvilinear relationship between ET_0 and UV-B irradiance for the original observations that can be well described by a 3rd degree polynomial (Fig. 7) and in a linear relationship between ET_0 and irradiance for longer wavelengths such as for blue light (Fig. 8).

To individually assess the performance of each variable as predictor of ET_0 we fitted first or third degree polynomials. Fig. 9 shows the adjusted R^2 from these fits, done separately for each month using data at 1 min intervals for sun elevation equal or more than five degrees. This shows, in agreement with the analysis in Fig. 2 that the best predictors are the various bands of sunlight, with

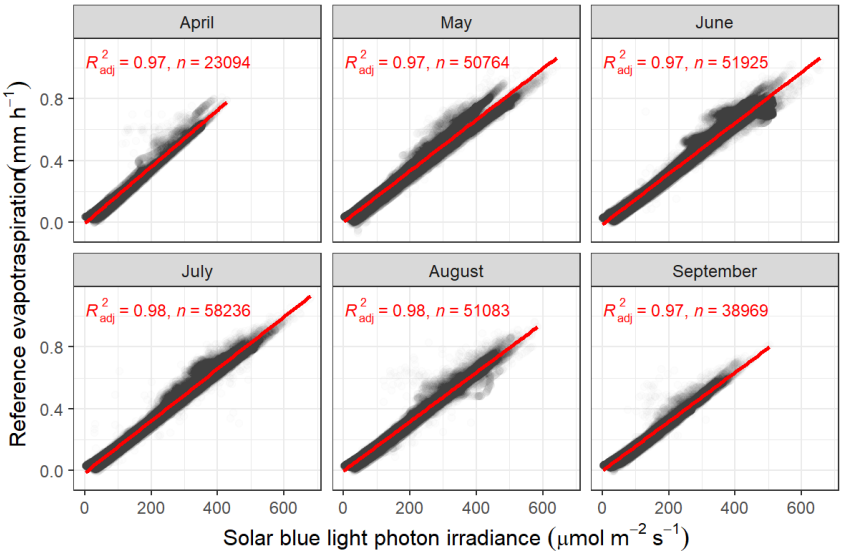

Figure 8: Relationship between reference evapotranspiration for a short vegetation cover (ET_0) vs. solar blue photon irradiance ($Q_{\text{UV-A}}$). Hourly averages computed from 60 values logged at 1 min interval. In red fitted linear regression. Observations are plotted as semi-transparent dots (black corresponds to 125 or more overlapping points). n = 274071.

PAR performing slightly better than UV radiation. Non-the-less even for UV-B radiation $R^2 > 0.85$ in all months (Fig. 7). In contrast, for VPD, the best performing of the variables not directly related to solar radiation, $0.24 > R^2 > 0.31$, i.e., $e^* - e$ explained in every case less than one third of the variation in ET_0 (Fig. 22).

A similar analysis for variation within the course of the photoperiod shows very high estimates of R^2 for all sunlight bands ($R^2 \geq 0.99$; Fig. 10). Of the remaining variables, wind is a good predictor of ET_0 during the photoperiod ($0.63 \leq R^2 \leq 0.91$). UV-B irradiance is a very good predictor of ET_0 even though the relationship is curvilinear (Fig. 20).

4. Discussion

Our analysis of the data highlights the importance of energy as the main driver of ET_0, and demonstrates that all bands of the solar spectrum are much better predictors of ET_0 than VPD, wind speed or T_{air}. The relationship between

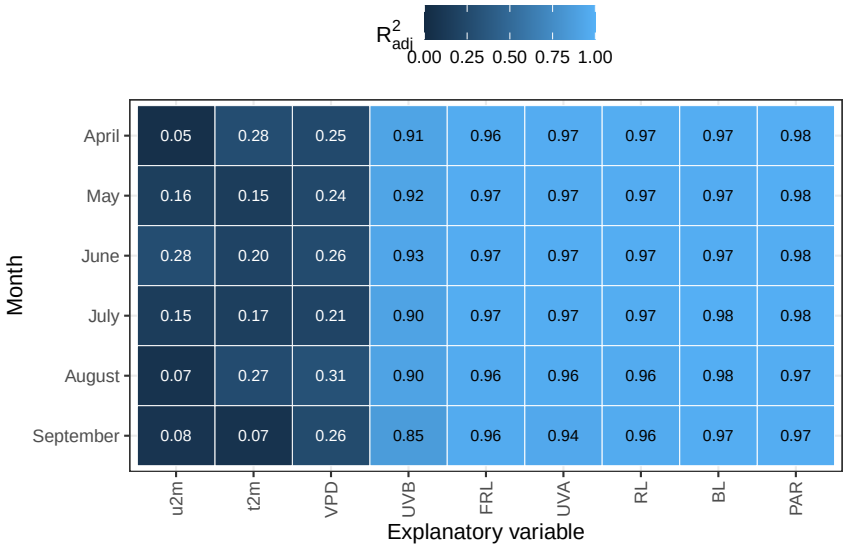

Figure 9: Adjusted R^2 for regressions of ET_0 on each of the variables individually, using observations and estimates for each minute. Data for sun elevation of 5 degrees or more during April to September. Explanatory variables are ordered along the x-axis according to their median R^2. The labels of the files are R^2 values. n = 274071.

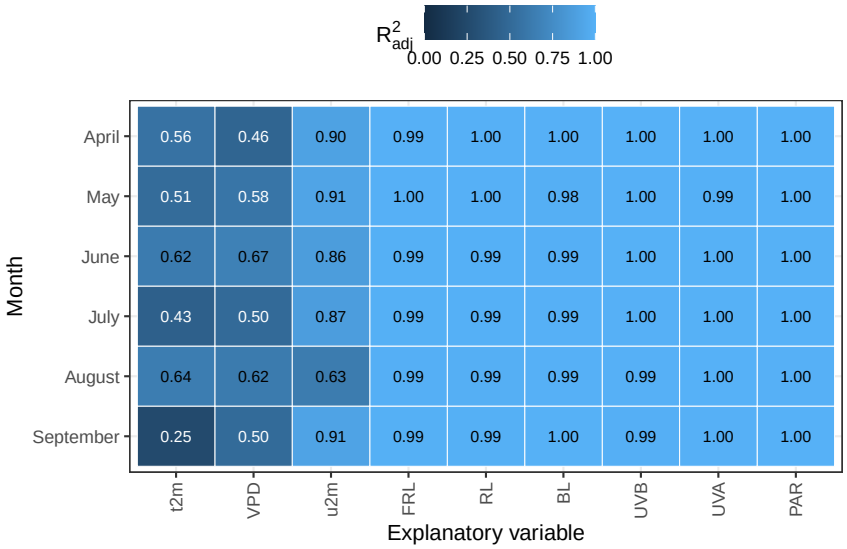

Figure 10: Adjusted R^2 for regressions of ET_0 on each of the variables individually, using monthly means for each hour of the photoperiod computed from observations and estimates for each minute. Data for sun elevation of 5 degrees or more during April to September. Explanatory variables are ordered along the x-axis according to their median R^2. The labels of the files are R^2 values. n = 275.

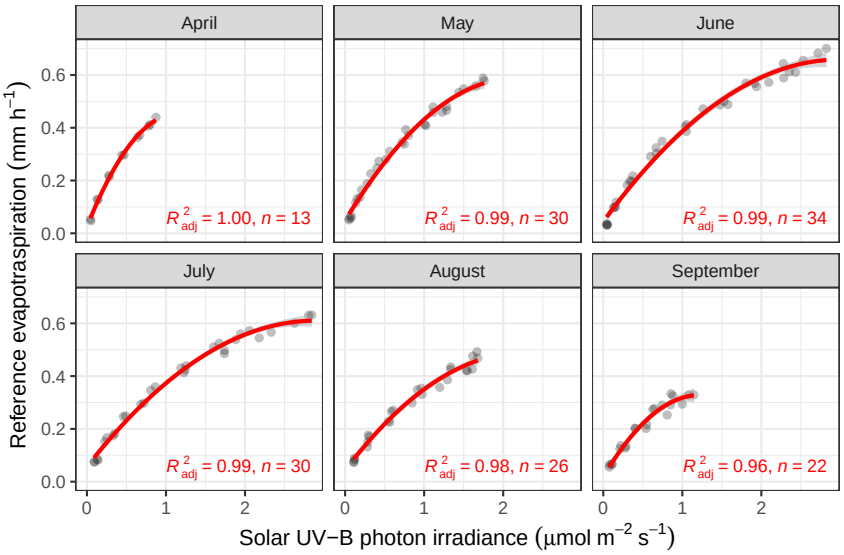

Figure 11: Relationship between reference evapotranspiration for a short vegetation cover (ET_0) vs. UV-B photon irradiance ($Q_{UV\text{-}B}$). Monthly averages computed for each hour of the photoperiod from values logged at 1 min interval. Data fron 2020 and 2021 averaged separately. Only values for sun elevation equal or higher to 5 degrees included. In red fitted 2nd degree polynomial.

down-welling short-wave radiation (I_{sw}) and irradiance in the blue (Q_B), red (Q_R) and far-red (Q_{FR}) regions is linear and very tight. In contrast, as $Q_{UV\text{-}B}$ has stronger dependency on solar elevation than I_{sw}, the relationship between them is curvilinear. They are also differently affected by clouds (Lindfors and Arola, 2008), possibly the reason for a relationship that is not as tight when considering day to day variation. In contrast, within the photoperiod there is little difference among wavebands in their performance as predictors.

Horizontal cosine corrected diffusers, as normally used, measure the radiation flux received on a horizontal surface (irradiance: I or Q). However, a horizontal plane is far from representing the true position of most plant leaves in a canopy. Diffusers with hemispherical or cylindrical shape could be used instead of flat ones and deployed both within and above canopies. So, an important *caveat* is that the irradiances we report here are not exactly the same as what individual plants and leaves are exposed when growing either in a canopy or isolated (Chelle, 2005).

Reference evapotranspiration, ET_0, is an abstraction that even if useful does not

describe the actual water loss from the soil (Campbell and Norman, 1998; Allen et al., 2006). Future studies assessing actual soil drying and water recharge, e.g., by measuring evapotranspiration with lysimeters, or by estimating it from soil volumetric water content and precipitation will allow to more precisely assess the information carried by cues. Measurements of the surface temperature of the canopy and long wave radiation would allow the use of equation (1) to validate estimates of ET.

There is evidence for a role of pre-exposure to UV-B and/or UV-A in preemptive acclimation to drought (e.g. Robson et al., 2016; Yan, 2021), but the usual explanation does not seem to hold, at least for our data set, as all wavebands of sunlight seem to function as cues carrying information about ET_0. This raises the question of why plants use UV exposure as a proxy informing about the likelihood of future drought. We propose three possible explanations as hypotheses for future studies: 1) UV exposure is a comparatively better predictor of ET_0 for plants growing within a canopy than when considering sunlight above a canopy; 2) irradiance measured on a horizontal plane may not represent what a plant senses; and 3) UV exposure in itself is a better predictor of future drought than ET_0.

Disentangling these questions has practical implications for crop breeding as it will explain under which conditions reductions in g_l^w contribute to population level water-use efficiency and under which conditions it does not. The albedo, LAI and timing of soil-water use can all affect canopy evapotranspiration, possibly as much or more than a decrease in g_l^w, while imposing different constraints and trade-offs on production. As far as we know, data like we are collecting at our station are not available anywhere else with a similarly high temporal resolution. A network of similar stations deployed worldwide would be very valuable for the development and deployment of precision agriculture. Thus, this report provides a starting point with respect to instrumentation and data analysis, in addition to answers to scientific questions.

References

Allen RG, **Pruitt WO**, **Wright JL**, et al. 2006. A recommendation on standardized surface resistance for hourly calculation of reference ETo by the FAO56 Penman-Monteith method. *Agricultural Water Management* 81. DOI: 10.1016/j.agwat.2005.03.007.

Aphalo PJ, **Albert A**, **Björn LO**, **McLeod AR**, **Robson TM**, **Rosenqvist E**, eds. 2012. *Beyond the Visible: A handbook of best practice in plant UV photobiology*. 1st ed. COST Action FA0906 "UV4growth". Helsinki: University of Helsinki, Department of Biosciences, Division of Plant Biology, xxx + 174. ISBN: 978-952-10-8363-1. DOI: 10.31885/9789521083631.

Aphalo PJ, **Ballaré CL**. 1995. On the importance of information-acquiring systems in plant-plant interactions. English. *Functional Ecology* 9, 5–14. DOI: 10.2307/2390084.

Aphalo PJ, **Jarvis PG**. 1991. Do stomata respond to relative humidity? *Plant, Cell and Environment* 14, 127–132. DOI: 10.1111/j.1365-3040.1991.tb01379.x.

Aphalo PJ, **Sadras VO**. 2021. *Explaining preemptive acclimation by linking information to plant phenotype*. DOI: 10.32942/osf.io/tvk5b.

Aphalo PJ. 2015. The r4photobiology suite. *UV4Plants Bulletin* 2015, 21–29. DOI: 10.19232/uv4pb.2015.1.14.

Aphalo PJ. 2021. *ggpmisc: Miscellaneous Extensions to 'ggplot2'*. https://CRAN.R-project.org/package=ggpmisc/.

Aphalo PJ, **Ylianttila L**. 2021. *ooacquire: Acquire Data from OO Spectrometers*. https://github.com/aphalo/ooacquire.

Aphalo PJ. 1991. Interactions in stomatal function. PhD thesis. University of Edinburgh.

Ballaré CL, **Scopel AL**, **Sánchez RA**. 1990. Far-red radiation reflected from adjacent leaves: an early signal of competition in plant canopies. *Science* 247, 329–332. DOI: 10.1126/science.247.4940.329.

Bandurska H, **Niedziela J**, **Chadzinikolau T**. 2013. Separate and combined responses to water deficit and UV-B radiation. *Plant Science* 213, 98–9105. ISSN: 0168-9452. DOI: 10.1016/j.plantsci.2013.09.003.

Buckley TN. 2005. The control of stomata by water balance. *New Phytol* 168, 275–292. DOI: 10.1111/j.1469–8137.2005.01543.x.

Campbell GS, **Norman JM**. 1998. *An Introduction to Environmental Biophysics*. English. 2nd ed. New York: Springer, 286. ISBN: 0-387-94937-2.

Capra F, **Luisi PL**. 2014. *The Systems View of Life*. Cambridge University Press. 514 pp. ISBN: 1316616436.

Casal JJ. 2013. Photoreceptor Signaling Networks in Plant Responses to Shade. *Annual Review of Plant Biology* 64, 403–427. DOI: 10.1146/annurev–arplant–050312–120221.

Casal JJ, **Qüesta JI**. 2018. Light and temperature cues: multitasking receptors and transcriptional integrators. *New Phytologist* 217, 1029–1034. DOI: 10.1111/nph.14890.

Chelle M. 2005. Phylloclimate or the climate perceived by individual plant organs: what is it? How to model it? What for? *New Phytol* 166, 781–790.

Durand M, **Matule B**, **Burgess AJ**, **Robson TM**. 2021. Sunfleck properties from time series of fluctuating light. *Agricultural and Forest Meteorology* 308-309, 108554. DOI: 10.1016/j.agrformet.2021.108554.

Gitz DC, **Liu-Gitz L**. 2003. How do UV photomorphogenic responses confer water stress tolerance? *Photochemistry and photobiology* 78, 529–534. DOI: 10.1562/0031–8655(2003)078<0529:HDUPRC>2.0.CO;2.

Grolemund G, **Wickham H**. 2011. Dates and Times Made Easy with lubridate. *Journal of Statistical Software* 40, 1–25. DOI: 10.18637/jss.v040.i03.

Grömping U. 2006. Relative Importance for Linear Regression in R: The Package relaimpo. *Journal of Statistical Software* 17, 1–27.

Hartikainen SM, **Pieristè M**, **Lassila J**, **Robson TM**. 2020. Seasonal Patterns in Spectral Irradiance and Leaf UV-A Absorbance Under Forest Canopies. *Frontiers in Plant Science* 10. DOI: 10.3389/fpls.2019.01762.

Hayes S, **Schachtschabel J**, **Mishkind M**, **Munnik T**, **Arisz SA**. 2021. Hot topic: Thermosensing in plants. *Plant, Cell & Environment* 44, 2018–2033. DOI: 10.1111/pce.13979.

Holmes MG. 1981. Spectral distribution of radiation within plant canopies. In: **H Smith**, ed. *Plants and the Daylight Spectrum*. London: Academic Press, 147–158.

Jarvis PG. 1985. Transpiration and assimilation of tree and agricultural crops: the 'Omega Factor'. In: **MGR Cannell**, **JE Jackson**, eds. *Attributes of Trees as Crop Plants*. Abbots Ripton: Institute of Terrestrial Ecology. Chap. 27, 460–480.

Jarvis PG, **McNaughton KG**. 1986. Stomatal Control of Transpiration: Scaling Up from Leaf to Region. *Advances in Ecological Research* 15, 1–49. DOI: 10.1016/s0065-2504(08)60119-1.

Kassambara A. 2019. *ggcorrplot: Visualization of a Correlation Matrix using 'ggplot2'*. R package version 0.1.3. URL: https://CRAN.R-project.org/package=ggcorrplot.

Kotilainen T, **Aphalo P**, **Brelsford C**, **Böök H**, **Devraj S**, **Heikkilä A**, **Hernández R**, **Kylling A**, **Lindfors A**, **Robson T**. 2020. Patterns in the spectral composition of sunlight and biologically meaningful spectral photon ratios as affected by atmospheric factors. *Agricultural and Forest Meteorology* 291, 108041. DOI: 10.1016/j.agrformet.2020.108041.

Lindfors A, **Arola A**. 2008. On the wavelength-dependent attenuation of UV radiation by clouds. *Geophysical Research Letters* 35, L05806. DOI: 10.1029/2007GL032571.

Lindfors AV, **Ylianttila L**. 2016. Visualizing Rayleigh scattering through UV photography. *Bulletin of the American Meteorological Society* 97, 1561–1564. DOI: 10.1175/bams-d-14-00260.1.

McNaughton KG. 1989. Regional interactions between canopies and the atmosphere. In: **G Russell**, **B Marshall**, **PG Jarvis**, eds. *Plant Canopies: Their Growth, Form and Function*. Vol. 31. Society for Experimental Biology Seminar Series. Cambridge: Cambridge University Press. Chap. 4, 63–82. DOI: 10.1017/cbo9780511752308.005.

Meeus J. 1998. *Astronomical Algorithms*. Willmann-Bell. ISBN: 0943396611.

Monteith JL. 1995. A reinterpretation of stomatal responses to humidity. *Plant, Cell and Environment* 18, 357–364. DOI: 10.1111/j.1365-3040.1995.tb00371.x.

Monteith J, **Unsworth M**. 2008. *Principles of Environmental Physics*. 3rd ed. Academic Press. ISBN: 0125051034.

Moriconi V, **Binkert M**, **Rojas MCC**, **Sellaro R**, **Ulm R**, **Casal JJ**. 2018. Perception of sunflecks by the UV-B photoreceptor UV RESISTANCE LOCUS 8. *Plant physiology*, pp–00048. DOI: 10.1104/pp.18.00048.

Mott KA, **Parkhurst DF**. 1991. Stomatal responses to humidity in air and helox. *Plant, Cell and Environment* 14, 509–515.

Müller K, **Wickham H**. 2021. *tibble: Simple Data Frames*. R package version 3.1.4. URL: https://CRAN.R-project.org/package=tibble.

Novoplansky A, **Cohen D**, **Sachs T**. 1990. How portulaca seedlings avoid their neighbors. *Oecologia* 82, 490–493. DOI: 10.1007/BF00319791.

Novoplansky A. 2016. Future Perception in Plants. In: **M Nadin**, ed. *Anticipation across disciplines*. Cognitive Systems Monographs. Berlin: Springer, 57–70. ISBN: 9783319225999. DOI: 10.1007/978-3-319-22599-9_5.

Paik I, **Huq E**. 2019. Plant photoreceptors: Multi-functional sensory proteins and their signaling networks. *Seminars in Cell & Developmental Biology*. DOI: 10.1016/j.semcdb.2019.03.007.

Peak D, **Mott KA**. 2011. A new, vapour-phase mechanism for stomatal responses to humidity and temperature. *Plant, cell & environment* 34, 162–178. DOI: 10.1111/j.1365-3040.2010.02234.x.

Pinheiro J, **Bates D**, **DebRoy S**, **Sarkar D**, **R Core Team**. 2021. *nlme: Linear and Nonlinear Mixed Effects Models*. R package version 3.1-152. URL: https://CRAN.R-project.org/package=nlme.

R Core Team. 2021. *R: A Language and Environment for Statistical Computing*. R Foundation for Statistical Computing. Vienna, Austria. URL: https://www.R-project.org/.

Rai N, **Morales LO**, **Aphalo PJ**. 2021. Perception of solar UV radiation by plants: photoreceptors and mechanisms. *Plant Physiology* 186, 1382–1396. DOI: 10.1093/plphys/kiab162.

Rai N, **O'Hara A**, **Farkas D**, et al. 2020. The photoreceptor UVR8 mediates the perception of both UV-B and UV-A wavelengths up to 350 nm of sunlight with responsivity moderated by cryptochromes. *Plant, Cell & Environment* 43, 1513–1527. DOI: 10.1111/pce.13752.

Robson TM, **Aphalo PJ**, **Banaś AK**, et al. 2019. A perspective on ecologically relevant plant-UV research and its practical application. *Photochemical & Photobiological Sciences* 18, 970–988.

Robson TM, **Hartikainen SM**, **Aphalo PJ**. 2016. How does solar ultraviolet-B radiation improve drought tolerance of silver birch (*Betula pendula* Roth.) seedlings? *Plant, Cell & Environment* 38, 953–967. DOI: 10.1111/pce.12405.

Smith H, ed. 1981a. *Plants and the Daylight Spectrum*. London: Academic Press. xx + 508.

Smith H. 1981b. Function, Evolution and Action of Plant Photosensors. In: **H Smith**, ed. *Plants and the Daylight Spectrum*. London: Academic Press, 499–508.

Smith H, **Morgan DC**. 1981. The spectral characteristics of the visible radiation Incident upon the surface of the Earth. In: **H Smith**, ed. *Plants and the Daylight Spectrum*. London: Academic Press, 3–20.

Song YH, **Shim JS**, **Kinmonth-Schultz HA**, **Imaizumi T**. 2015. Photoperiodic Flowering: Time Measurement Mechanisms in Leaves. *Annual Review of Plant Biology* 66, 441–464. DOI: 10.1146/annurev-arplant-043014-115555.

Telewski FW. 2006. A unified hypothesis of mechanoperception in plants. *American Journal of Botany* 93, 1466–1476.

Tissot N, **Ulm R**. 2020. Cryptochrome-mediated blue-light signalling modulates UVR8 photoreceptor activity and contributes to UV-B tolerance in Arabidopsis. 11. DOI: 10.1038/s41467-020-15133-y.

Wickham H. 2016. *ggplot2*. Springer International Publishing. DOI: 10.1007/978-3-319-24277-4.

Wickham H. 2021. *tidyr: Tidy Messy Data*. R package version 1.1.4. URL: https://CRAN.R-project.org/package=tidyr.

Wickham H, **François R**, **Henry L**, **Müller K**. 2021. *dplyr: A Grammar of Data Manipulation*. R package version 1.0.7. URL: https://CRAN.R-project.org/package=dplyr.

Yan Y. 2021. Long-term exposure to solar blue and UV radiation in legumes : pre-acclimation to drought and accession-dependent responses in two successive generations. English. PhD thesis. Helsinki: University of Helsinki, Faculty of Biological and Environmental Sciences. ISBN: 978-951-51-6933-4. URL: https://urn.fi/URN:ISBN:978-951-51-6933-4. visited on 05/30/2021.

Ylianttila L, **Visuri R**, **Huurto L**, **Jokela K**. 2005. Evaluation of a single-monochromator diode array spectroradiometer for sunbed UV-radiation measurements. *Photochemistry and Photobiology* 81, 333–341. DOI: 10.1111/j.1751-1097.2005.tb00192.x.

A. Supplementary Material

A.1. Daily totals and means

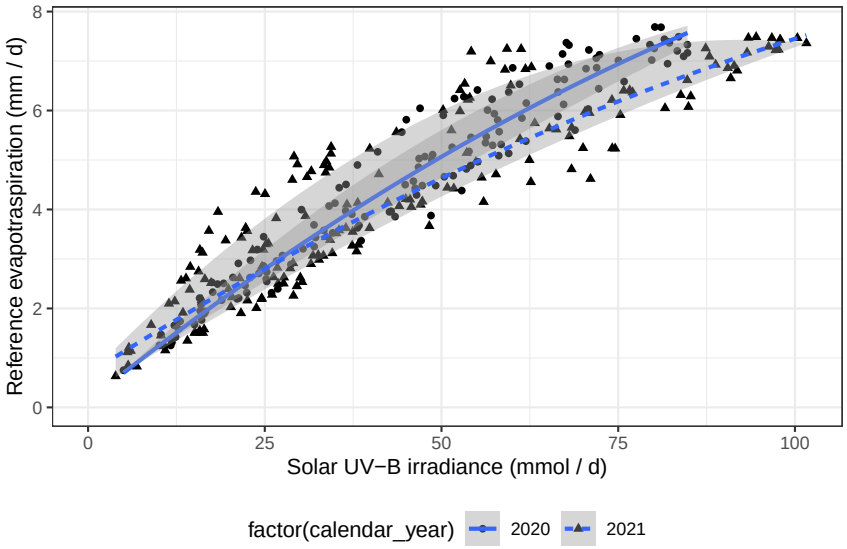

Figure 12: Relationship between reference evapotranspiration for a short vegetation cover (ET_0) and UV-B photon irradiance ($Q_{\text{UV-B}}$). Monthly averages computed for each hour of the photoperiod from values logged at 1 min interval. Median regression (line) and quartile regressions (band), second degree polynomials.

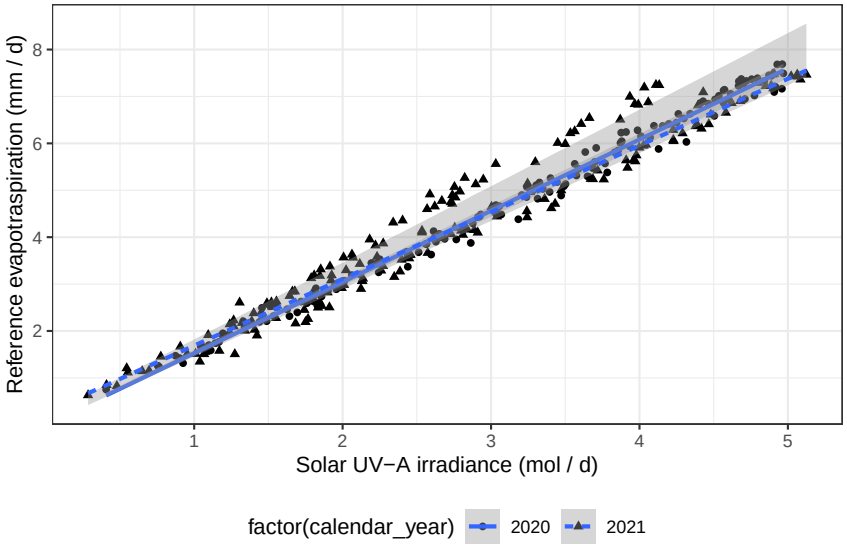

Figure 13: Relationship between reference evapotranspiration for a short vegetation cover (ET_0) and UV-A photon irradiance ($Q_{UV\text{-}A}$). Monthly averages computed for each hour of the photoperiod from values logged at 1 min interval. Median regression (line) and quartile regressions (band), first degree polynomial.

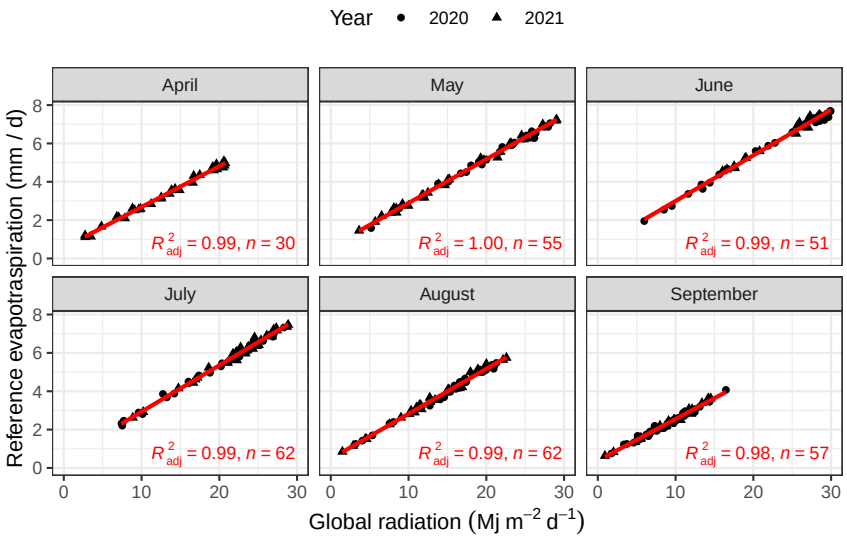

Figure 14: Relationship between reference evapotranspiration for a short vegetation cover (ET_0) vs. global radiation (H_{sw}). Daily sums computed from 1 440 values logged at 1 min interval. In red fitted 2nd degree polynomial.

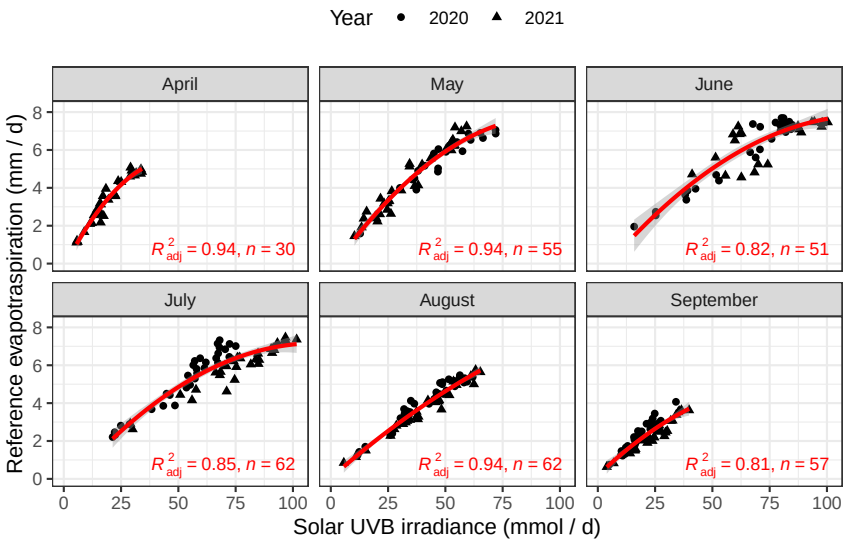

Figure 15: Relationship between reference evapotranspiration for a short vegetation cover (ET_0) vs. UV-B photon exposure ($H_{UV\text{-}B}$). Daily sums computed from 1 440 values logged at 1 min interval. In red fitted 2nd degree polynomial.

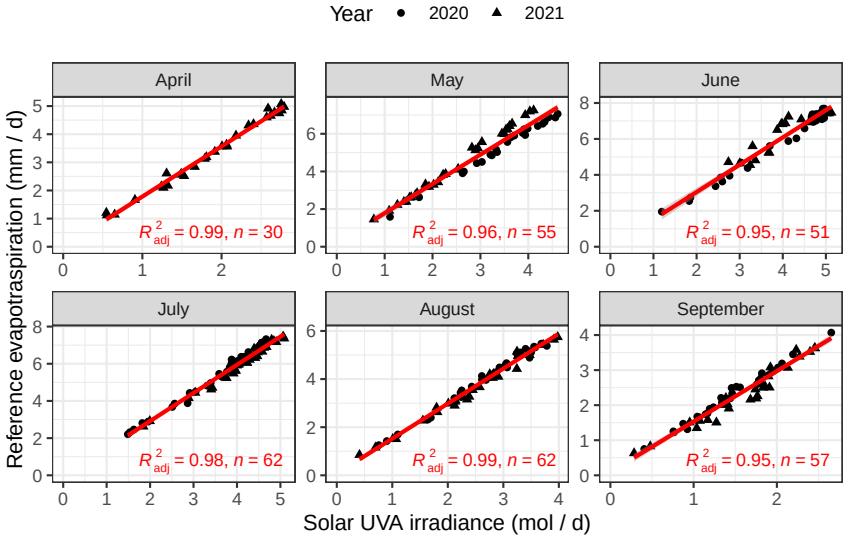

Figure 16: Relationship between reference evapotranspiration for a short vegetation cover (ET_0) vs. UV-A photon exposure ($H_{UV\text{-}A}$). Daily sums computed from 1 440 values logged at 1 min interval. In red fitted 2nd degree polynomial.

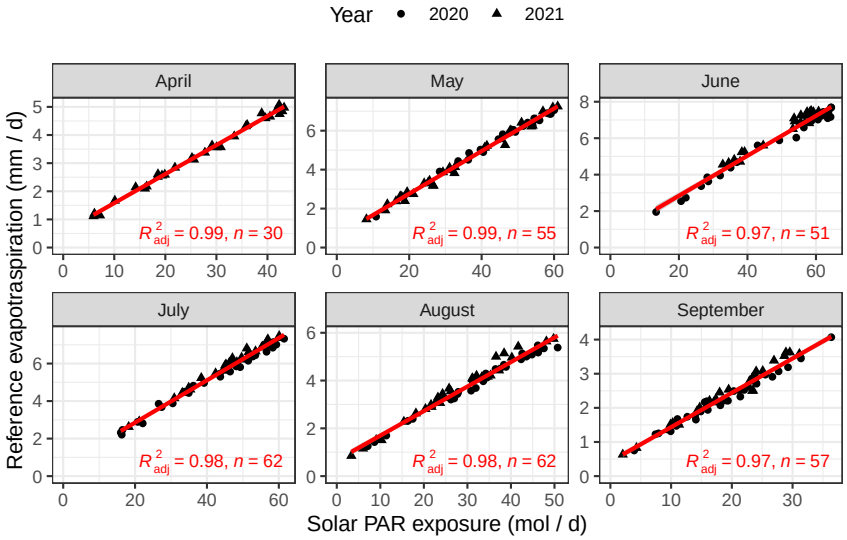

Figure 17: Relationship between reference evapotranspiration for a short vegetation cover (ET_0) vs. PAR photon exposure ($H_{UV\text{-}A}$). Daily sums computed from 1 440 values logged at 1 min interval. In red fitted 2nd degree polynomial.

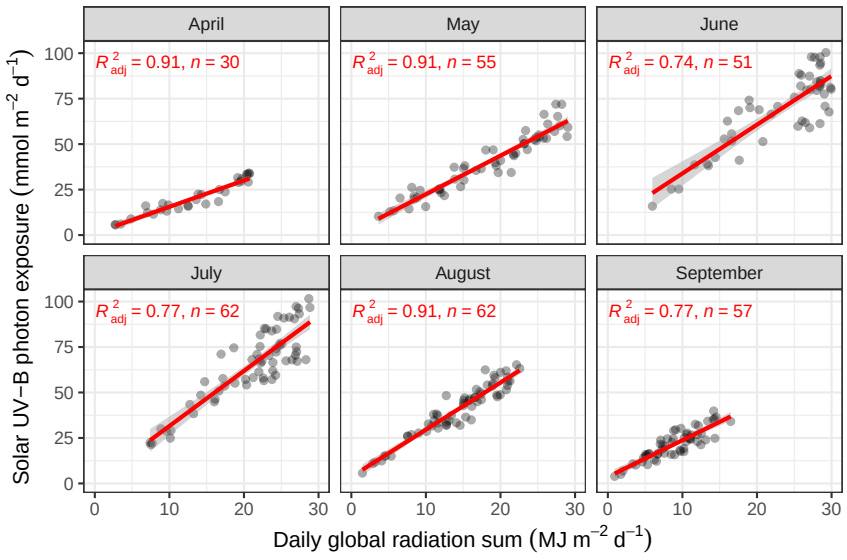

Figure 18: Short-wave radiation (H_{sw}) vs. UV-B photon exposure ($H_{UV\text{-}B}$). Daily sums computed from 1 440 values logged at 1 min interval. In red fitted 1st degree polynomial.

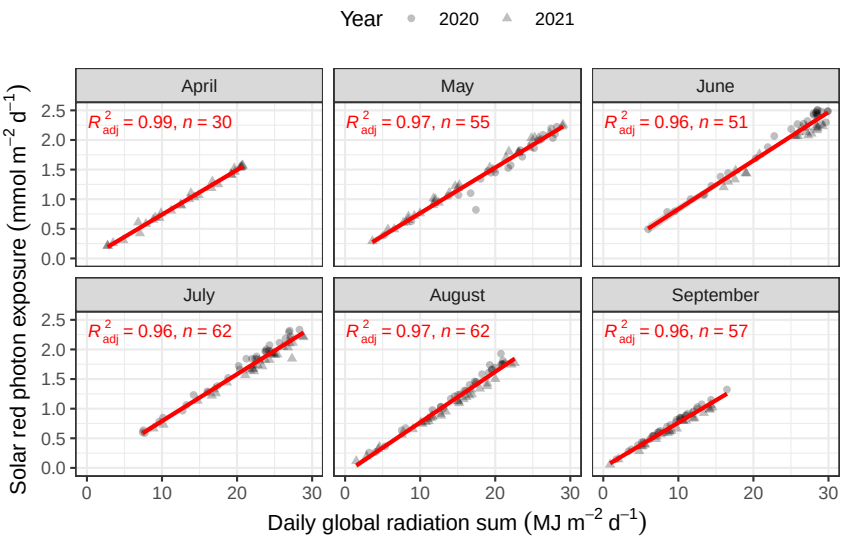

Figure 19: Short-wave radiation (H_{sw}) vs. red photon exposure (H_R). Daily sums computed from 1 440 values logged at 1 min interval. In red fitted 1st degree polynomial.

A.2. Variation within the photoperiod

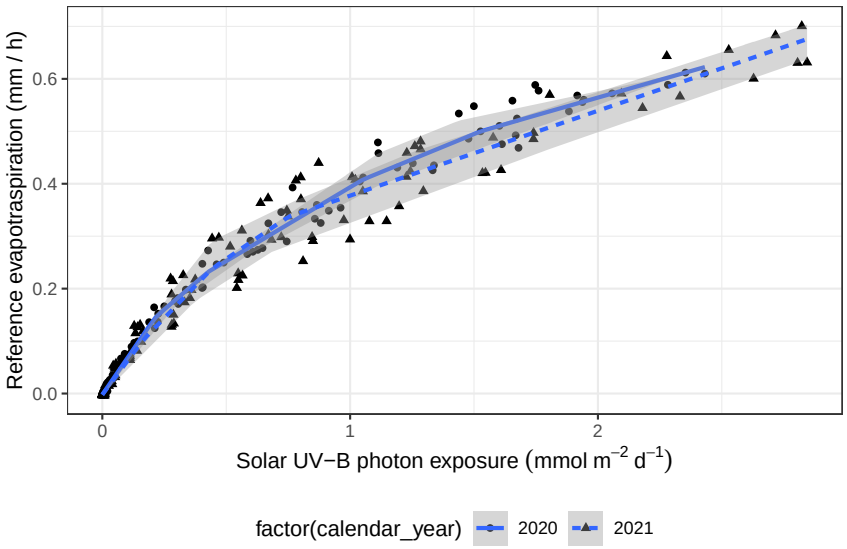

Figure 20: Relationship between reference evapotranspiration for a short vegetation cover (ET_0) and UV-B photon irradiance ($Q_{\text{UV-B}}$). Monthly averages computed for each hour of the photoperiod from values logged at 1 min interval. Median regression (line) and quartile regressions (band) using a spline.

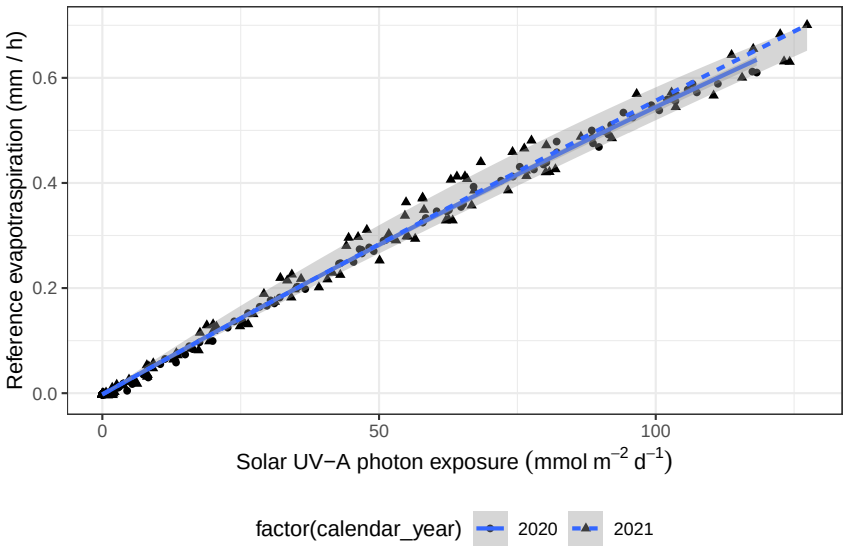

Figure 21: Relationship between reference evapotranspiration for a short vegetation cover (ET_0) and UV-A photon irradiance ($Q_{UV\text{-}A}$). Monthly averages computed for each hour of the photoperiod from values logged at 1 min interval. Median regression (line) and quartile regressions (band), second degree polynomial.

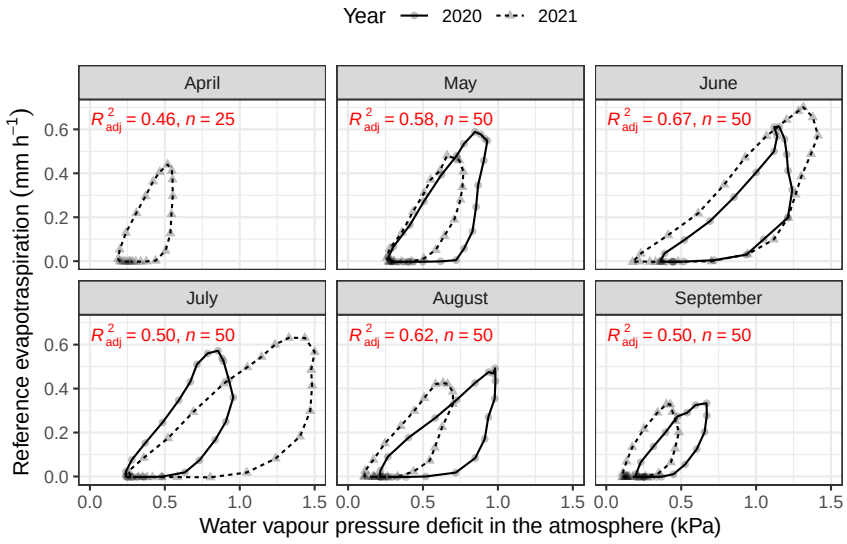

Figure 22: Average daily path of the relationship between reference evapotranspiration for a short vegetation cover (ET_0) vs. water vapour pressure deficit ($e^* - e$). Monthly averages computed for each hour of the photoperiod from values logged at 1 min interval.

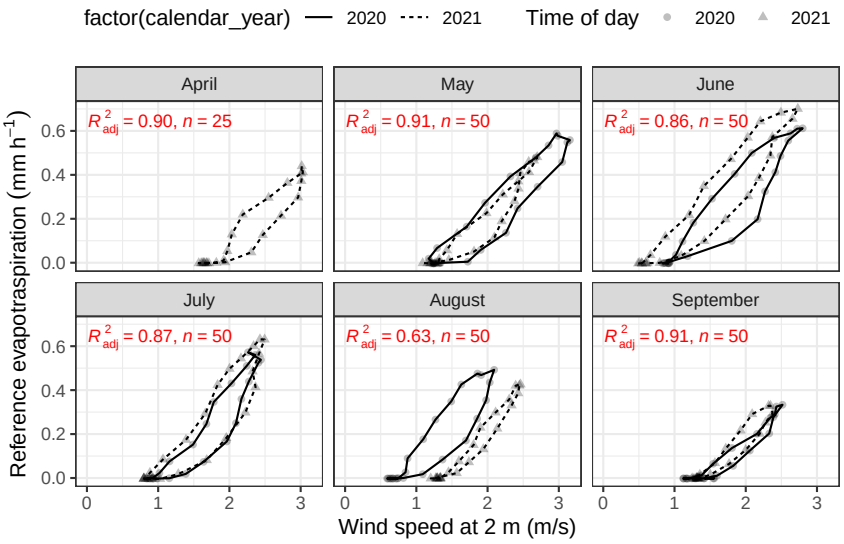

Figure 23: Average daily path of the relationship between reference evapotranspiration for a short vegetation cover (ET_0) vs. water vapour pressure deficit ($e^* - e$). Monthly averages computed for each hour of the photoperiod from values logged at 1 min interval.

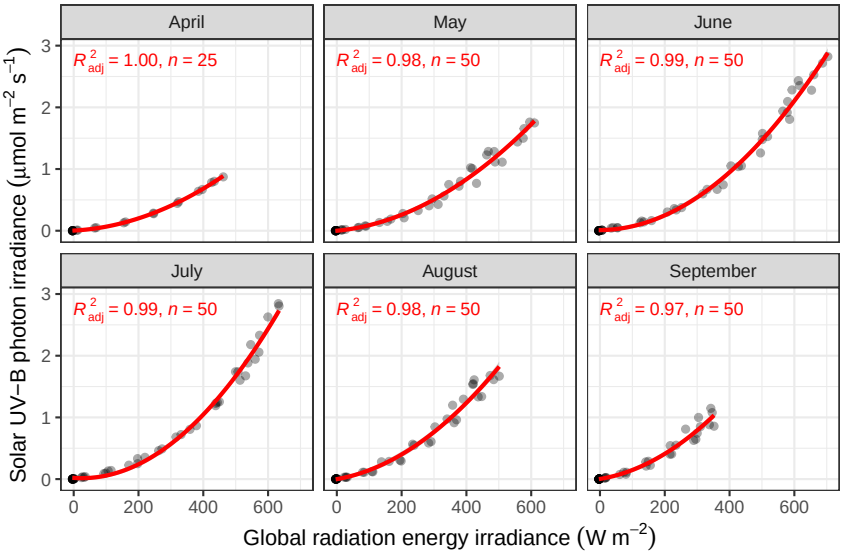

Figure 24: Short-wave global energy irradiance (I_{sw}) vs. UV-B photon irradiance ($Q_{UV\text{-}B}$). Monthly averages computed for each hour of the photoperiod from values logged at 1 min interval. In red fitted 2nd degree polynomial.

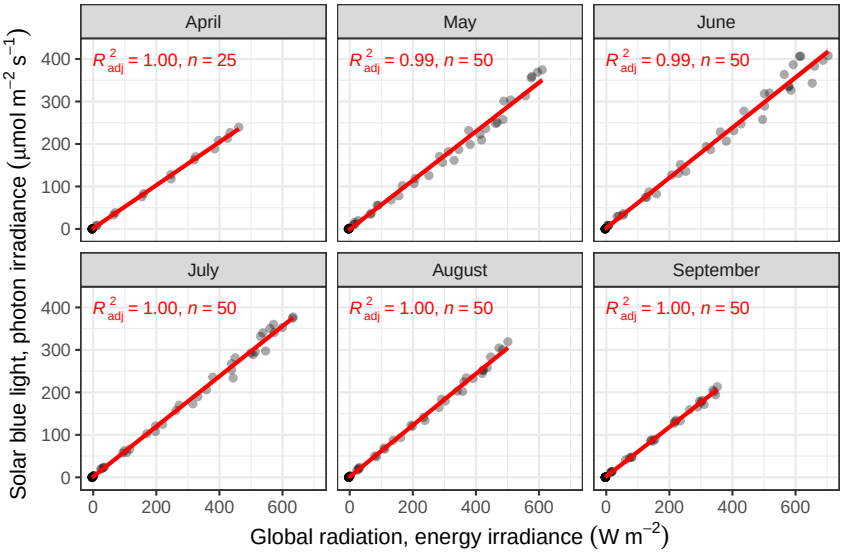

Figure 25: Short-wave global energy irradiance (I_{sw}) vs. R photon irradiance (Q_R). Monthly averages computed for each hour of the photoperiod from values logged at 1 min interval. In red fitted linear regression.